NASA/TM—2006-214430

Experimental Results of Thin-Film Photovoltaic Cells in a Low Density LEO Plasma Environment: Ground Tests

Joel T. Galofaro
Glenn Research Center, Cleveland, Ohio

Boris V. Vayner
Ohio Aerospace Institute, Brook Park, Ohio

November 2006

NASA STI Program . . . in Profile

Since its founding, NASA has been dedicated to the advancement of aeronautics and space science. The NASA Scientific and Technical Information (STI) program plays a key part in helping NASA maintain this important role.

The NASA STI Program operates under the auspices of the Agency Chief Information Officer. It collects, organizes, provides for archiving, and disseminates NASA's STI. The NASA STI program provides access to the NASA Aeronautics and Space Database and its public interface, the NASA Technical Reports Server, thus providing one of the largest collections of aeronautical and space science STI in the world. Results are published in both non-NASA channels and by NASA in the NASA STI Report Series, which includes the following report types:

- TECHNICAL PUBLICATION. Reports of completed research or a major significant phase of research that present the results of NASA programs and include extensive data or theoretical analysis. Includes compilations of significant scientific and technical data and information deemed to be of continuing reference value. NASA counterpart of peer-reviewed formal professional papers but has less stringent limitations on manuscript length and extent of graphic presentations.

- TECHNICAL MEMORANDUM. Scientific and technical findings that are preliminary or of specialized interest, e.g., quick release reports, working papers, and bibliographies that contain minimal annotation. Does not contain extensive analysis.

- CONTRACTOR REPORT. Scientific and technical findings by NASA-sponsored contractors and grantees.

- CONFERENCE PUBLICATION. Collected papers from scientific and technical conferences, symposia, seminars, or other meetings sponsored or cosponsored by NASA.

- SPECIAL PUBLICATION. Scientific, technical, or historical information from NASA programs, projects, and missions, often concerned with subjects having substantial public interest.

- TECHNICAL TRANSLATION. English-language translations of foreign scientific and technical material pertinent to NASA's mission.

Specialized services also include creating custom thesauri, building customized databases, organizing and publishing research results.

For more information about the NASA STI program, see the following:

- Access the NASA STI program home page at *http://www.sti.nasa.gov*

- E-mail your question via the Internet to *help@sti.nasa.gov*

- Fax your question to the NASA STI Help Desk at 301–621–0134

- Telephone the NASA STI Help Desk at 301–621–0390

- Write to:
  NASA STI Help Desk
  NASA Center for AeroSpace Information
  7121 Standard Drive
  Hanover, MD 21076–1320

NASA/TM—2006-214430

Experimental Results of Thin-Film Photovoltaic Cells in a Low Density LEO Plasma Environment: Ground Tests

Joel T. Galofaro
Glenn Research Center, Cleveland, Ohio

Boris V. Vayner
Ohio Aerospace Institute, Brook Park, Ohio

Prepared for the
Fourth World Conference on Photovoltaic Energy Conversion
sponsored by the Institute of Electrical and Electronics Engineers
Waikoloa, Hawaii, May 7–12, 2006

National Aeronautics and
Space Administration

Glenn Research Center
Cleveland, Ohio 44135

November 2006

Acknowledgments

The authors would like to express their gratitude to the Air Force Research Laboratory (AFRL) in bringing this manuscript to publication. A special thanks to Pawel Tlomak AFRL and Michael Piszczor, Jr., NASA Glenn Research Center, for their helpful dialogue and timely communications regarding the entire publication process.

Level of Review: This material has been technically reviewed by technical management.

Available from

NASA Center for Aerospace Information
7121 Standard Drive
Hanover, MD 21076–1320

National Technical Information Service
5285 Port Royal Road
Springfield, VA 22161

Available electronically at http://gltrs.grc.nasa.gov

Experimental Results of Thin-Film Photovoltaic Cells in a Low Density LEO Plasma Environment: Ground Tests

Joel T. Galofaro
National Aeronautics and Space Administration
Glenn Research Center
Cleveland, Ohio 44135

Boris V. Vayner
Ohio Aerospace Institute
Brook Park, Ohio 44142

Abstract

Plasma ground testing results, conducted at the Glenn Research Center (GRC) National Plasma Interaction (N-PI) Facility, are presented for a number of thin-film photovoltaic cells. The cells represent a mix of promising new technologies identified by the Air Force Research Laboratory (AFRL) under the CYGNUS Space Science Technology Experiment (SSTE-4) Program. The current ground tests are aimed at characterizing the performance and survivability of thin film technologies in the harsh low earth orbital space environment where they will be flown. Measurements of parasitic current loss, charging/dielectric breakdown of cover-slide coatings and arcing threshold tests are performed for each individual cell. These measurements are followed by a series of experiments designed to test for catastrophic arc failure mechanisms. A special type of power supply, called a solar array simulator (SAS) with adjustable voltage and current limits on the supply's output, is employed to bias two adjacent cells at a predetermined voltage and current. The bias voltage is incrementally ramped up until a sustained arc results. Sustained arcs are precursors to catastrophic arc failure were the arc current rises to a maximum value for long timescales (often ranging between 30 to 100 μsec times). Normal arcs by comparison, are short lived events with a timescale between 10 to 30 μs. Sustained arcs lead to pyrolization with extreme cell damage and have been shown to cause the loss of entire array strings in solar arrays. The collected data will be used to evaluate the suitability of thin-film photovoltaic technologies for future space operations.

Introduction

The basic circuit element in all spacecraft photovoltaic (PV) power generation systems is configured from a number of solar cells connected in series forming a single string element. The entire array is then composed from a number of such identical string elements. The number of strings connected in series provides the full operational potential for the array; the number of strings connected in parallel provides the maximum operating current for the array. Several arrays are often connected to form a single wing and a typical spacecraft may have one or more wings making up its power generation system. Batteries are often employed to store power during times when the array is in full darkness (eclipse). The PV arrays, the reserve capacity of the batteries, the power distribution network and power management software all combine to define the overall robustness of the power system.

The negative end of the solar array and batteries are typically grounded to the spacecraft structure, thereby providing a single point ground connection. It is the negative grounding scheme, coupled with the spacecraft structure and plasma environment, that is responsible for all related array/spacecraft interactions with the orbital plasma environment (refs. 1 to 6). While cell composition and physical layout do play important roles, they are not the most important factors in determining how the array and spacecraft structure interact the plasma environment. The single most important factor in determining the magnitude of the interactions with the space plasma environment lies with the designed operating potential or the design voltage of the spacecraft power system. Due to low mass and volume stowage limitations imposed by current solar cell technologies, the maximum on-orbit power supplied by the

current generation photovoltaic arrays is limited to only about 30 kW of power (ref. 7). A new generation of TFPV solar cell technologies seeks to overcome the mass and stowage limitations imposed by current day cell technologies. To that end a number of promising TFPV cell technologies are tested to see how they perform in a low density space plasma environment.

A test plan was hammered out at the GRC/AFRL meeting in an early February of 2005. Originally the Air Force Research Laboratory (AFRL) had planned on conducting a plasma test on sixty sample coupons. Due to time and cost constraints the number of samples to be tested was reduced down to a more manageable number at the February meeting. The first order discussion entailed the need to test the cells as close as possible to their actual flight configuration. It was decided that the backside of the cells needed to be exposed to the plasma, just as they would be deployed in space. A matter of some conjecture was the need for a standardized way of testing solar cell samples. First the solar cells needed a rigid support to protect them from damage during evacuation and venting operations in the chamber. Furthermore, in order to avoid large deviations in the measured cell efficiency, both the contact and wire resistance are standardized using the same fixed length cable for all cells mounted on the test fixture. The outputs leads from each cell were connected using coaxial RG58U cables terminated with standard male type BNC connectors. The cable and cell contact points were then insulated to prevent them from arcing in the space plasma. AFRL contracted a major aerospace company to build the actual test fixture hardware, to mount the cells on the test fixture and to make all coaxial cable output connections to the cells. Two large test fixtures, with an area of approximately one square meter, arrived at the facility for testing in early September. The first test fixture was populated with a mix of nine sample coupons provided by three different solar cell manufactures (fig. 1(a) to (d)). The nine sample coupons comprised state of the art TFPV technologies of both amorphous silicon (a-Si) and Copper Indium Gallium Diselenide (CIGS) cells. A second test fixture populated with six a-Si cells from the same manufacturer was also supplied for testing (fig. 2(a) to (d)). The two test fixtures represent the most promising light weight TFPV technologies identified to date by the AFRL.

Experimental Setup

Plasma tests were performed in the 1.8 m long by 1.8 m diameter test section inside the Teney vacuum chamber geosynchronous (GEO) charging simulator (fig. 3(a)). The Teney chamber is capable of both Low Earth Orbit (LEO) and GEO operations. The vacuum system is backed by a holding pump and a 0.9 m (36 in.) diameter cryo-tub. The first test fixture (containing nine sample test coupons) was suspended at the far end the chamber (fig. 3(b)). The cells were electrically floated with respect to tank ground. Separate connections were made for each cells output leads using high voltage electrical feedthrough's mounted on a large port located on the tank wall. A Penning type discharge source (mounted on the vacuum side of the tank door) ionizes a controlled flow of xenon gas neutrals flowing past a hot filament in magnetic field. The plasma source is electrically floated in the chamber with a positive bias being applied between the positive case anode and negative filament cathode. All measured tank pressures were obtained using an ionization gage. The arcing monitor detection system consists of a simple R-C circuit (fig. 3), a voltage probe, current probes, current probe amplifiers and a 4 channel 400 Mhz oscilloscope (fig. 3(c)). The R-C circuit is used to bias the cell relative to the plasma just as it would be in space. The circuit is used to simulate the arcing conditions for cells by dumping an equivalent amount of charge from the capacitor that represents the total spacecraft capacitance. Typical spacecraft capacitances range from 1 to 4 μF. A capacitance value, C = 1 μF was used for all arcing tests. A Software driven oscilloscope control program arms the scope, puts it in a wait condition awaiting a change in state in the trigger signal. Once the oscilloscope is triggered, the control program instructs the scope to dump all waveform data from memory to non volatile disk storage. The control program proceeds to rearm the scope and awaits the next trigger event. Other equipment includes a color camera for imaging arcs, a DVD video recorder, color TV monitor, two programmable power supplies (source measure units), a solar array simulator power supply with adjustable voltage and current limits, and a quadrupole mass spectrometer for identifying gas species inside the chamber.

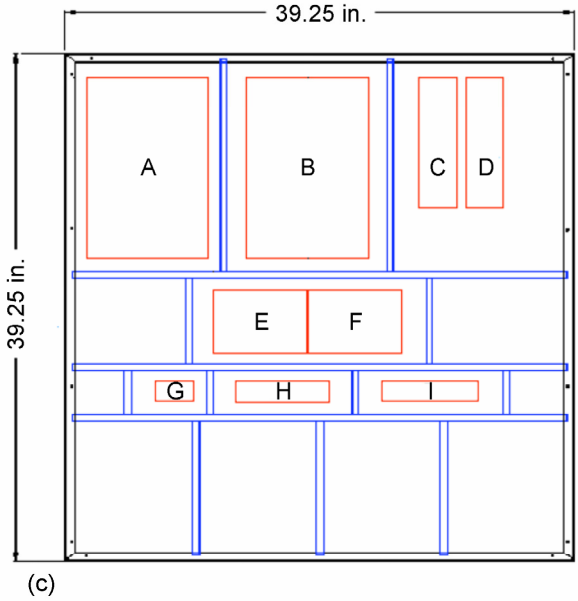

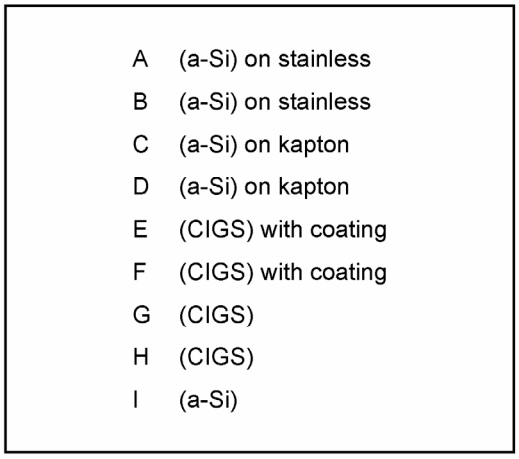

Figure 1.—(a) Front facing view of completed test fixture (RG58U) with male BNC connectors). (b) Back facing view of test fixture with rigid cell support structure and stainless blanket. (c) Block diagram showing cell placement and cell. (d) Legend key illustrating cell technology.

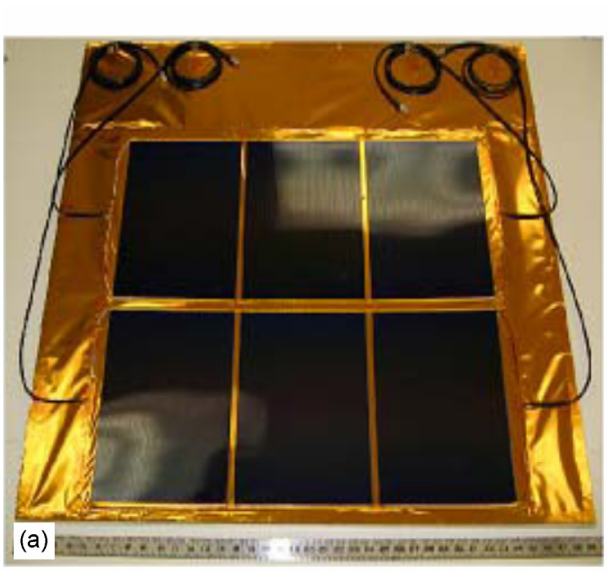

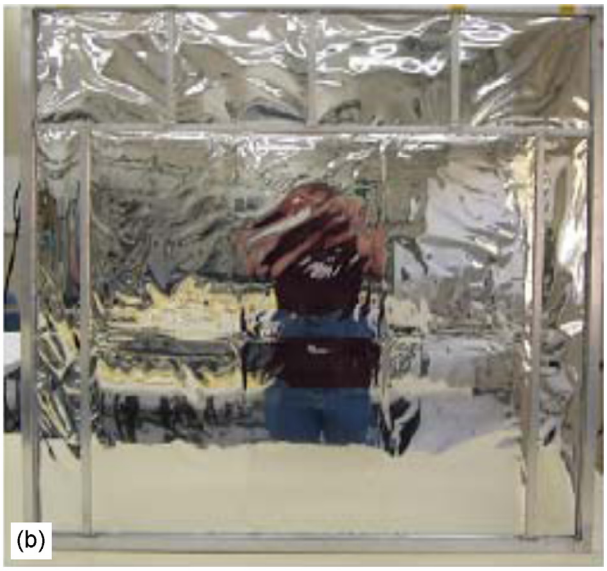

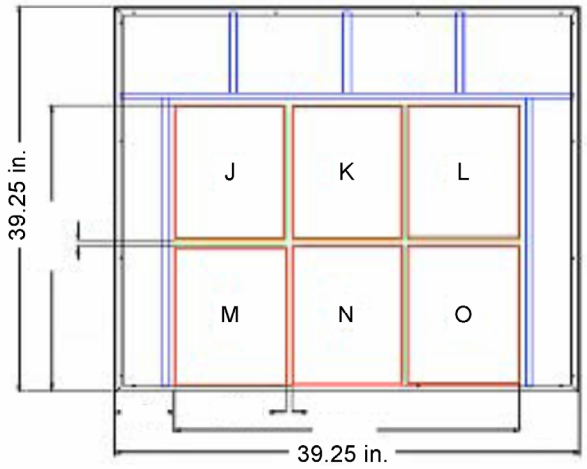

(c)

Circuit A string cells:

J (a-Si) on stainless

K (a-Si) on stainless

L (a-Si) on stainless

Circuit B string cells:

M (a-Si) on stainless

N (a-Si) on stainless

O (a-Si) on stainless

(d)

Figure 2.—(a) Front facing view of completed test fixture and cells. String circuit A: cells J, K and L. (b) Back facing view of test fixture with rigid cell support structure and stainless blanket. (c) Block diagram detailing cell location. (d) Legend indicating cell technology.

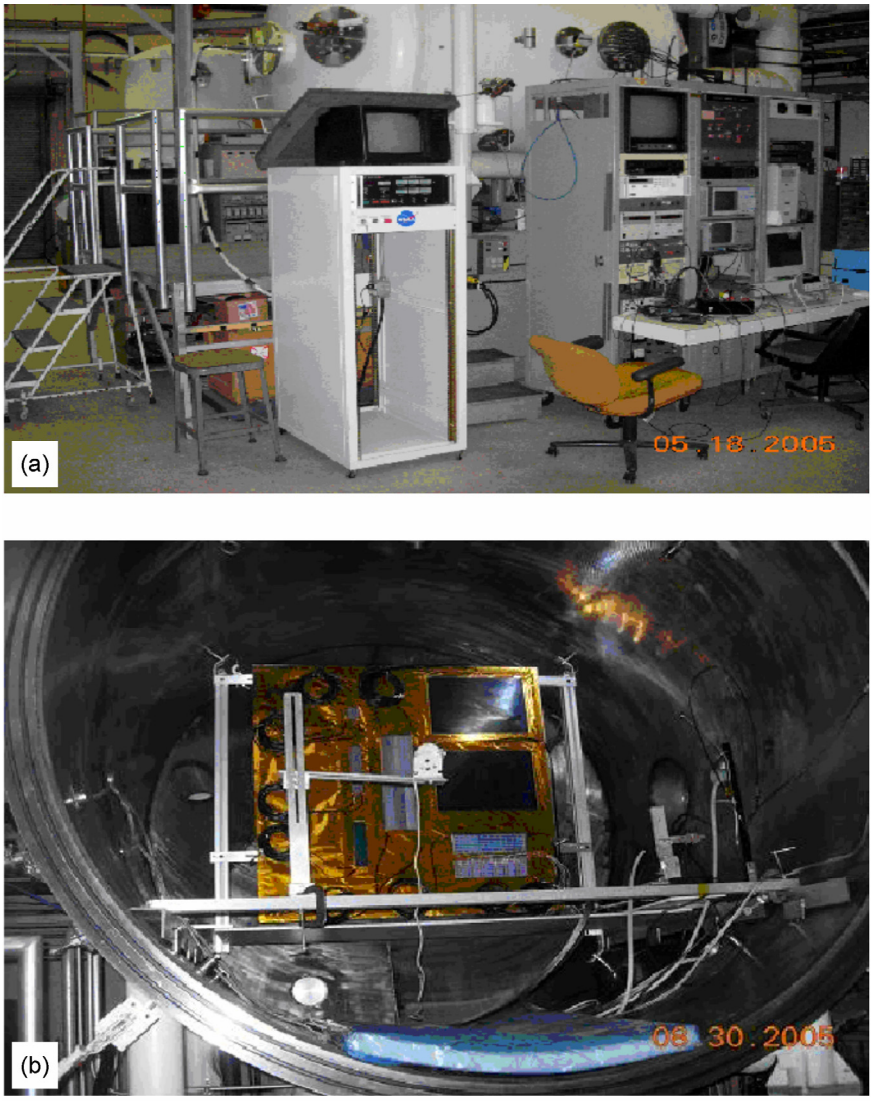

Figure 3.—(a) Teney Geosynchronous Charging Simulator. The addition of a xenon plasma source allows LEO simulations to be run in tandem. (b) Snapshot of first test fixture mounted inside chamber. Cells were outgassed for 24 hours under hard vacuum before testing. (c) R-C circuit and equipment used for capturing arc waveform data. Illustrated setup was used in all cell arcing tests. (d) Experimental setup used for sustained arcing tests. The same setup is used for both LEO and GEO environments.

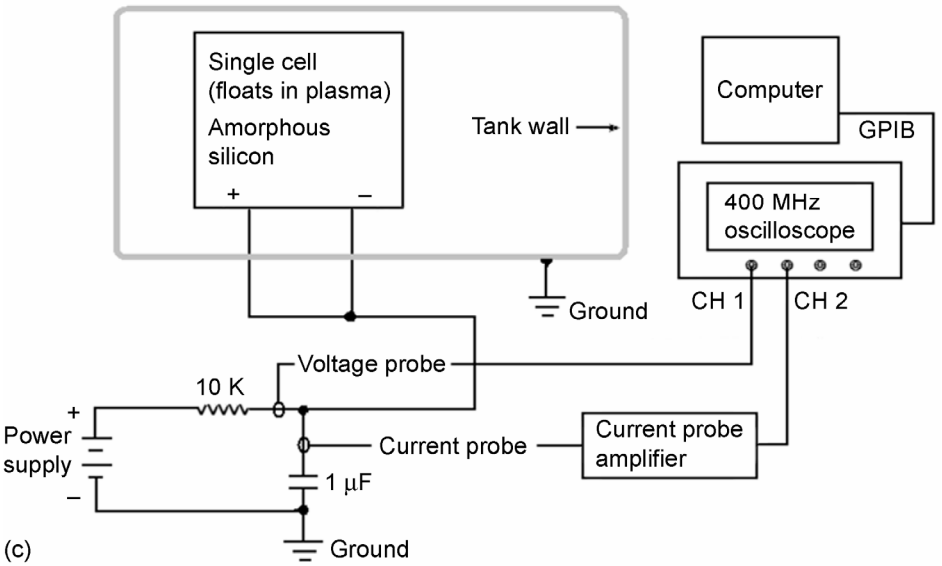

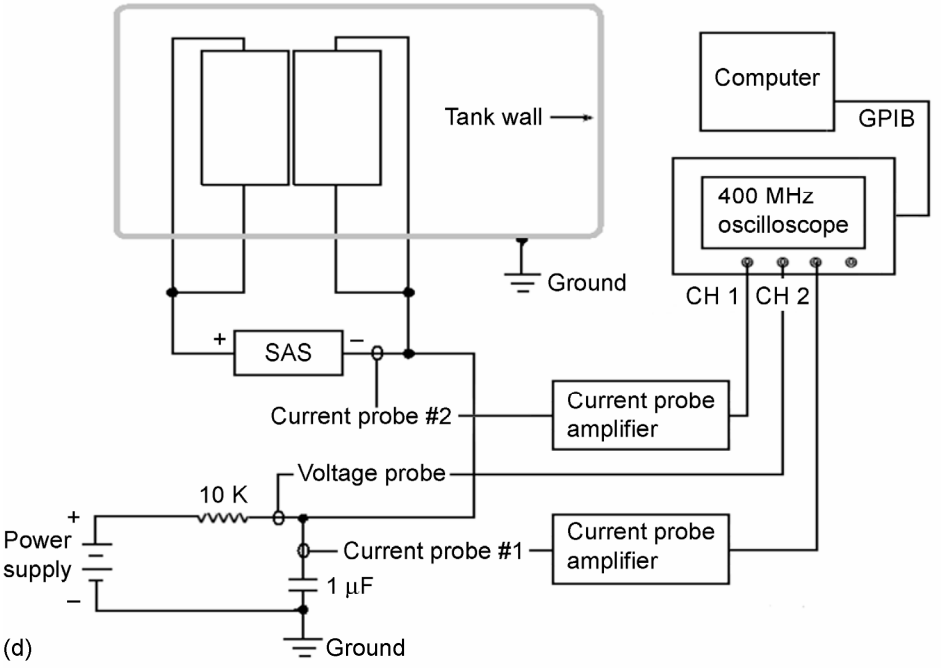

Figure 3.—Concluded. (c) R-C circuit and equipment used for capturing arc waveform data. Illustrated setup was used in all cell arcing tests. (d) Experimental setup used for sustained arcing tests. The same setup is used for both LEO and GEO environments.

Experimental Results

Prior to any plasma testing in the Teney vacuum chamber both test fixtures were delivered to the PV solar array simulator lab for characterization. As a control, a first round of baseline measurements were made in air under full illumination (1 sun) using a high power UV arc lamp. Measurements of short circuit current (Isc), open circuit voltage (Voc), maximum current (Imax), maximum voltage (Vmax), maximum power (Pmax) and cell efficiency (Eff %) were obtained for each cell on both test fixtures.

The first test fixture was returned back to N-PIF in the beginning of September and installed inside the Teney vacuum chamber. Solar cell samples were allowed to outgas for 48 hr at the base pressure, $P = 2.2\times10^{-7}$ torr, prior to plasma testing. A pressure reading $P = 1.1\times10^{-5}$ torr was maintained during tests with the xenon plasma source operating. A floating spherical Langmuir probe was sweep through a range of potentials to obtain the volt-ampere characteristic curve. Applying standard reduction techniques, to the experimentally obtained curve, yielded the following xenon plasma parameters: Floating potential, $V_f = 0.5$ V, Plasma potential, $V_p = 7.4$ V, electron temperature, $T_e = 0.38$ eV and electron number density, $N_e = 5.4\times10^5$ electrons per cubic centimeter.

In order to simulate the cell interactions with the LEO plasma environment the cells are electrically floated in the chamber and immersed in the xenon plasma. The output leads of each cell are shorted together and negatively biased with a programmable power supply located outside the chamber. Parasitic current collection of a cell is a measure quality of insulator material of the cell. Large parasitic currents in the space plasma tend reduce the overall rated output power generated by the cell. In order to get a better understanding of the effect of parasitic current loss a current collection curve (voltampere curve) is obtained in-situ for each cell. (fig. 4(a) to (d)). Note that coupon D shown in figure 1(a) and (c) is actually composed of six separate a-Si cells labeled Da, Db, Dc, Dd, De, Df. Due to electrical breakdown and

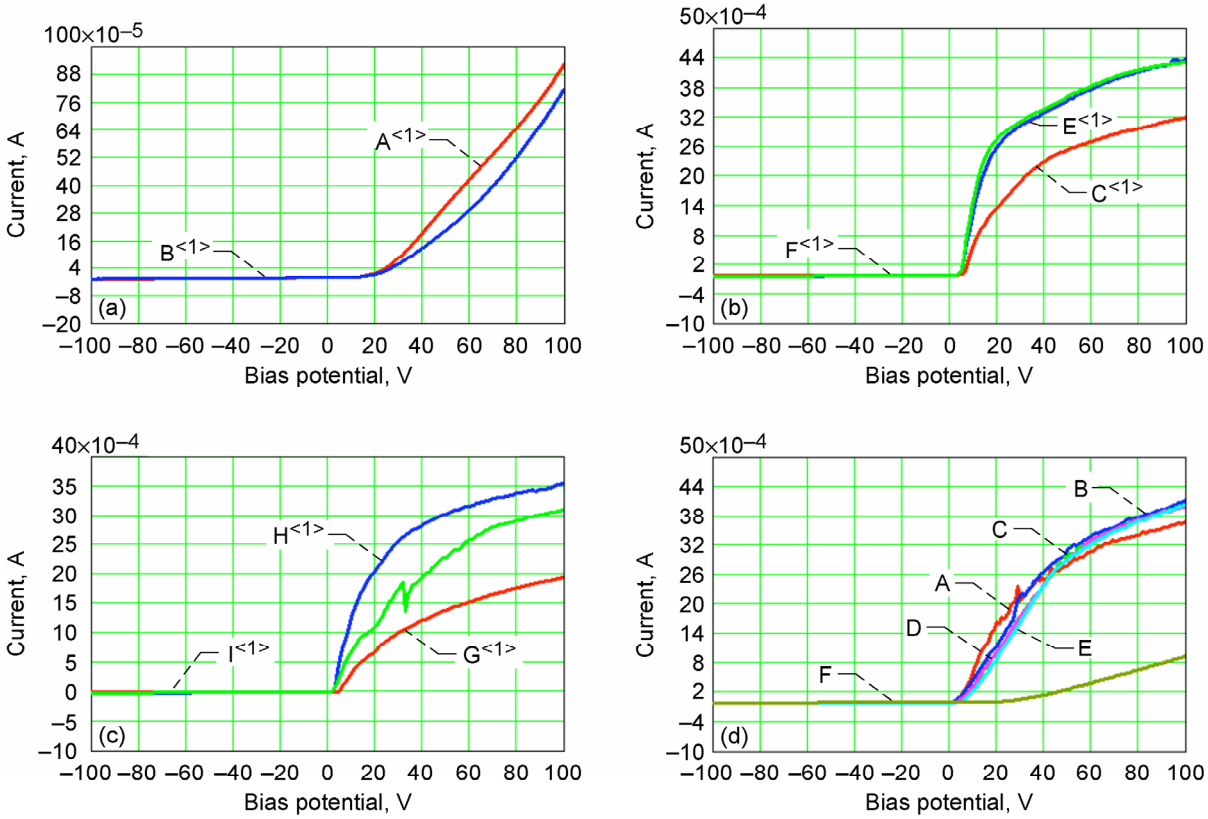

Figure 4.—(a) Current collection curve for (a-Ai) cells on stainless. (A = 25 micron thick, B = 10 micron thick coating). (b) Current collection results for (CIGS) cells E and F and (a-Si) cell C. (c) Current collection results for (CIGS) cells G and H and (a-Si) cell I. (d) Current collection results for six individual (a-Si) cell on cell D.

subsequent and surface flashing concerns the voltage has been limited to bias voltages between –100 and 100 V. The scaled parasitic current values shown in table A have been recalculated based on all cells having the same area.

TABLE A.—SCALED PARASITIC CURRENT RESULTS

Coupon	Area [cm^2]	Scale factor	Current [A]
Cell A	816	1	9.2709e–004
Cell B	816	1	8.2099e–004
Cell C	168	4.9	1.5766e–002
Cell Da	14	58.3	2.1472e–001
Cell Db	14	58.3	2.4060e–001
Cell Dc	14	58.3	2.3597e–001
Cell Dd	14	58.3	2.3451e–001
Cell De	14	58.3	2.3574e–001
Cell Df	14	58.3	5.4742e–002
Cell E	180	4.5	1.9705e–002
Cell F	180	4.5	1.9449e–002
Cell G	17.5	46.6	9.0707e–002
Cell H	63	12.9	4.5805e–002
Cell I	68	12	3.7220e–002

The next set of plasma experiments involved obtaining the arcing threshold of each cell. Arcing threshold is determined by negatively biasing each cell (through an R-C network, fig. 3(c)) and counting the number of arc events occurring in a predetermined time interval. If no arcs are observed at a given potential at the end of the time interval the bias level is increased and the test is repeated for the next time interval. The point at which arcs are first recorded determines the arcing threshold of the cell. To get a better handle on the maximum cell voltage encountered in orbit, each cell needs to be tested at the most negative potential developed by the cell in space. The most negative cell potential is actually specified by the designed operating voltage of the power system, which for the current tests is 280 V. Assuming a designed operating voltage, V_{op} = 280 V, and using the values of V_f = 0.5 V and V_p = 7.4 V specified earlier, the power system should float at a potential, V_F = –273.1 V. (eq. (1)). In order to provide a large safety margin against catastrophic cell failure (encountered during times of severe geomagnetic substorm activity) it was decided to bias individual cells up to a maximum potential of –400 V (with the exception

$$V_F = \left(V_p - V_f\right) - V_{op} \tag{1}$$

to cell D which tested up to –450 V). The results obtained from the arcing tests are summarized in table B. There appears to be two different kinds of arcs: one that is triggered normally and the one that appears as a surface flash with no trigger. Non-triggered arcs appear to be caused by micro discharges in the dielectric insulating layer. Because micro discharges are small by definition, they often occur well below the trigger level set on the current probe.

To gain a better understanding of the mechanism behind such discharges, two different current probes (high current and low current) were employed, with the scope being triggered at a level set by the low current probe. Experience has shown that arcs (and maybe micro discharges) are often caused by absorbed water vapor at the triple junction sites on solar arrays (refs. 8 to 11). Micro discharges occurring in the surface layer are not large enough to cause the full charge stored in the capacitor to be discharged as in the case of an arc. A surface flash appears to generate micro discharges on the order of 70 mA of current (fig. 5(a) and (b) for details). Micro discharges occurring in the insulating layer of the film may however be considered as precursors to full fledged arcs. A question arose concerning the accumulated damage effects micro discharges (surface flashes) have on the long term survivability of dielectric insulator coatings in space. To help answer the coating survivability question a 1 hr long test was run at a sustained bias level of –170 V (with a 1 μF capacitor in parallel) on the large a-Si sample on cell A. The

arc rate appeared to slow down considerably after a large initial number of surface flashing events (99 flashes) with no apparent visual degradation to the coating of the cell (see time lapse in fig. 6).

TABLE B.—ARCING RATES RECORDED AT INDICATED BIAS LEVEL
(SSF = Single Surface Flash, MCF = Multiple Surface Flashes)

Coupon	Bias level [V]	Arc rate [no./15 min]	Comments
Cell A	–100	1	
	–150	0	
	–170	MSF	scope not triggered
	–200	MSF	scope not triggered
Cell B	–125	1	
	–150	4	
	–150	5	
Cell C	–100	5	
	–125	4	
Cell Da	–150	14	
	–200	5	
	–250	4	
Cell Db	–450	SSF	no trigger
Cell Dc	–450	1	
Cell Dd	–450	0	
Cell De	–450	0	
Cell Df	–450	0	
Cell E	–100	2	
	–125	11	per minute
	–150	8	
Cell F	–100	2	
	–125	4, MSF	flashes not triggered
Cell G	–350	1, SSF	1 trigger arc, 1 SSF
	–400	4	
Cell H	–300	2	
	–350	6	6 arcs in 5 min
Cell I	–350	5	

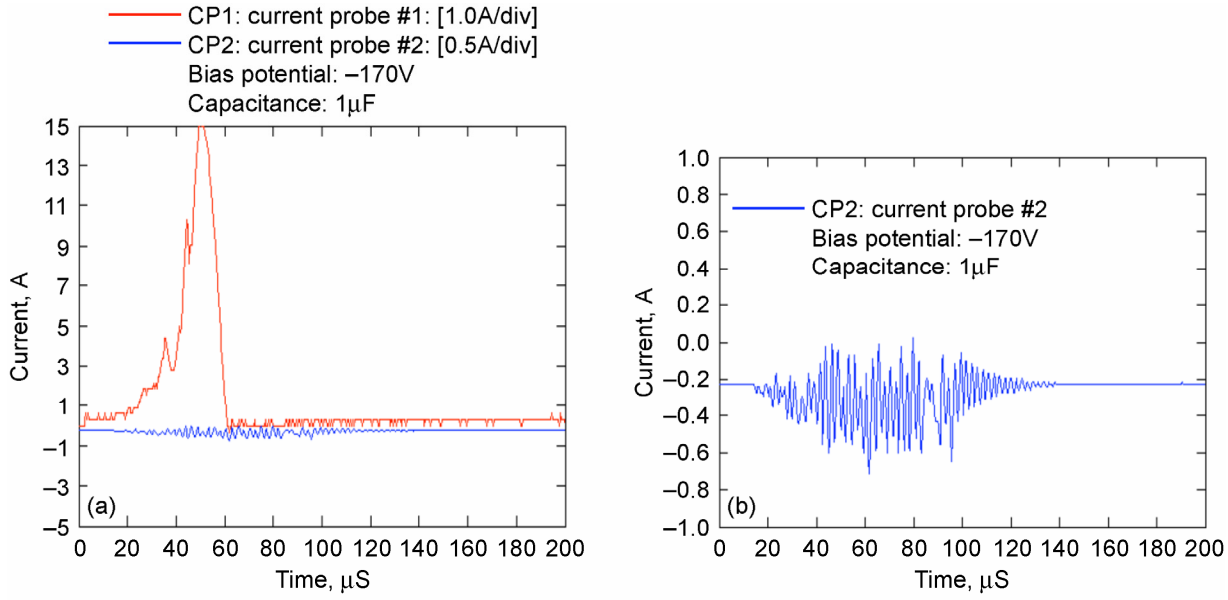

Figure 5.—(a) Example of a triggered arc and micro discharge (flash) plotted on the same scale. (b) Same micro discharge (flash) in figure (5a) but plotted in greater detail.

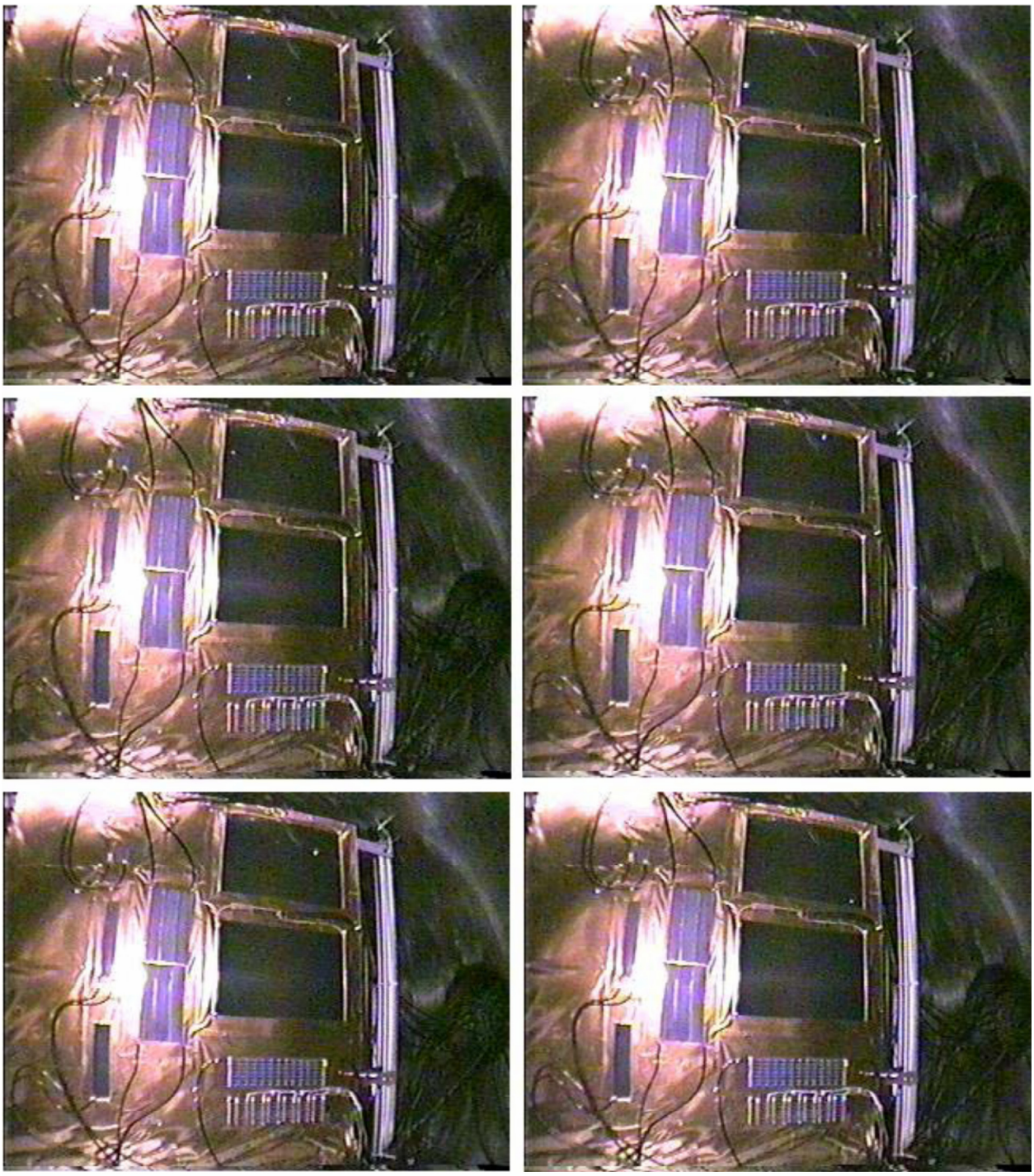

Figure 6.—Time lapse showing several flashes recorded during first 10 seconds. Bias potential –170V, capacitance 1 μF.

Another way of characterizing the cell is to determine how much voltage the cell is able to standoff without undergoing electrical breakdown. Electric field (E-field) strength is a direct measure of the how much voltage a given cell is able to withstand without arcing. An upper limit on the E-field strength can be estimated if the thickness z of the dielectric coating and the bias voltage ϕ at which the cell undergoes electrical breakdown is known. The magnitude of E-field strength can be estimated from the formulations given in equations 2(a) to (d). The E-field strength has dimensions of V/m and can be calculated directly from equation 2(d). Note that the E-field strength is measured in the z direction which is taken to be normal to the face of the cell.

$$\left\| \vec{E} \cdot \hat{k} \right\| = \left\| -grad\,\phi \cdot \hat{k} = -\left(\frac{\partial \phi_x}{\partial x}\hat{i} + \frac{\partial \phi_y}{\partial x}\hat{j} + \frac{\partial \phi_z}{\partial z}\hat{k} \right) \cdot \hat{k} \right\| \tag{2a}$$

Where: $\vec{E}$ is the electric field vector and $\hat{i}$, $\hat{j}$, $\hat{k}$ are unit normal vectors and

$$\left\| \vec{E} \cdot \hat{k} \right\| = \left\| -\left(\frac{\partial \phi_x}{\partial x}\hat{i} \cdot \hat{k} + \frac{\partial \phi_y}{\partial y}\hat{j} \cdot \hat{k} + \frac{\partial \phi_z}{\partial z}\hat{k} \cdot \hat{k} \right) \right\| = \frac{\partial \phi_z}{\partial z} \tag{2b}$$

$$\left\| \vec{E} \cdot \hat{k} \right\| = \frac{\partial \phi_z}{\partial z} = \frac{\phi - \phi_o}{z - z_o} \tag{2c}$$

Letting: $\phi = 0$ and $z_o =$ yields

$$\left\| \vec{E} \cdot \hat{k} \right\| = \frac{\phi}{z} \tag{2d}$$

Thus, critical field strength can be estimated as 100 V/25 μm = 4 MV/m for cell A and as 25 V/10 μm = 12.5 MV/m for the cell B.

Sustained arcing tests were then run in a LEO environment on samples E and F (fig. 1(a) to (c)). The solar array simulator (SAS) was then placed between the shorted outputs of cells E and F (see fig. 3(d) for details). Cell E was attached to the negative end of the SAS and the positive end of the SAS was connected to cell F. Sample E was initially biased at –200 V and a SAS voltage of 120 V (with both 1 and 2 A current limit settings) was used during the tests. Several triggered arc events were recorded between cells along with multiple surface flashes that were not triggered. No sustained arcs were observed during any of the tests. See figure 7(a) for further details. After SAS testing a current collection curve was run for samples E and F. The current collection results are shown in figure 7(b). The entire test fixture was then removed from the chamber and delivered to the PV solar array flash simulator lab for retesting in air.

The second test fixture was installed in the chamber and both strings were allowed to outgas in the chamber for 48 hr under hard vacuum. The plasma source was then placed in an operational mode and adjusted until the same plasma conditions for the previous tests were met. A current collection curve was obtained on Strings 1 and 2. See figure 8(a) for details. Parasitic current results indicated that both Strings 1 and 2 collected more current than the virgin samples.

Next sustained arcing tests were performed on Strings 1 and 2 using the setup shown in figure 3(d). Note that String 1 consists of three a-Si cells (J, K, and L) wired in series and String 2 is made up of three similar a-Si cells (M, N, and O) also wired in series (see figure 2(a) and (b) for details). Several measurements were initially performed with String 1 biased at –170 V with the negative end of the SAS being connected to String 1 and the positive end of the SAS connected to String 2. A SAS output voltage

of 120 V with a 2 A current limit was set for the sustained arc tests. Several trigger arc events were recorded, along with multiple surface flashing events that were not triggered. The SAS output connections to Strings 1 and 2 were then reversed. String 1 was connected to positive end of the SAS and the negative SAS end was connected to String 2. An output SAS voltage of 120 V with a 2 A current limit was used and several triggered and non-triggered arc events arc events were recorded. Figure 8(b) shows typical triggered response recorded during this part of the tests. No sustained arcs were observed for any of the tests run between Strings 1 and 2. A final round of cell performance measurements were then obtained in air on the second test fixture with mixed results. See table C for further details.

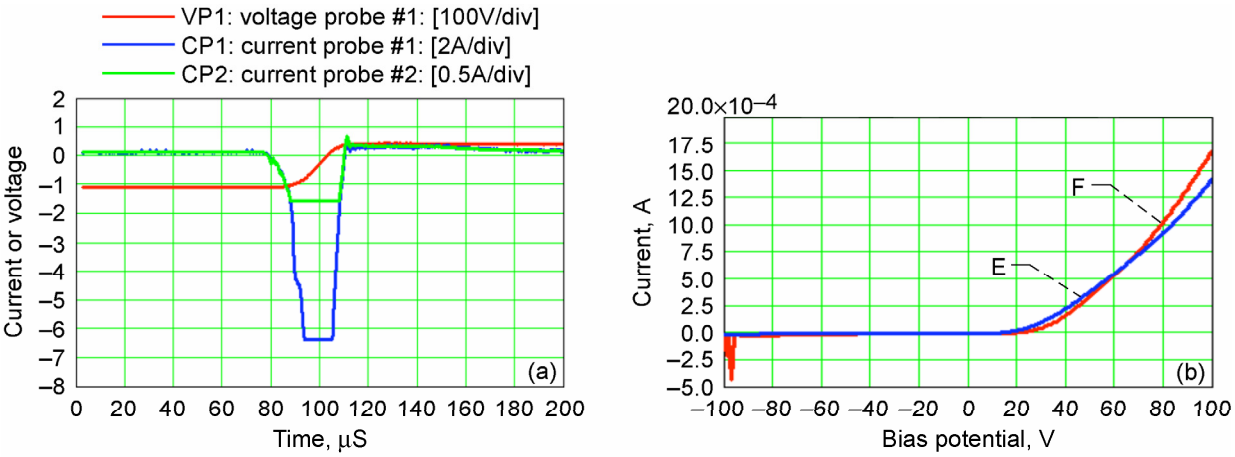

Figure 7.—(a) SAS test between cells E and F. Typical waveforms acquired for sustained arcing test. Note that pulse width of CP1 and CP2 exactly match indicating no sustained arcs detected. (b) Collection current plot for cell E and F. SAS not biased.

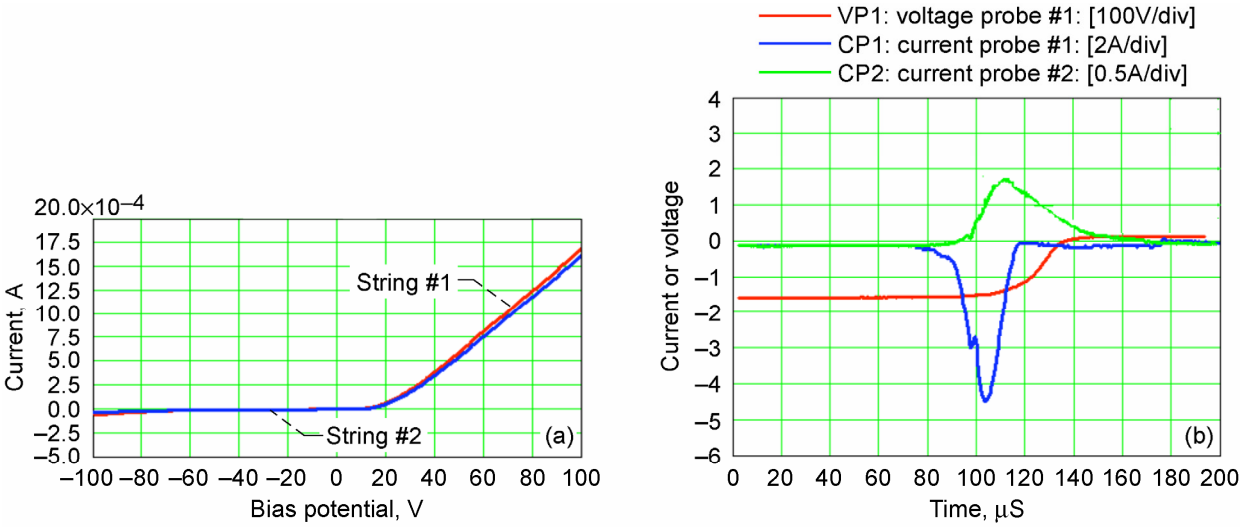

Figure 8.—(a) Current collection plot for strings #1 and #2. SAS not biased. (b) Typical arc recorded between strings with + SAS tied to string #1 and –SAS tied to string #2. Recorded waveform illustrates that current pulse widths (CP1 and CP2) are extended but since the current level of CP2 drops back to zero the arc is not sustained.

TABLE C.—REPORTED CHANGE IN EFFICIENCY AFTER PLASMA TESTING. PV SIMULATOR PERFORMANCE TEST IN AIR WITH FULLE (1 SUN) SOLAR UV IRRADIANCE SPECTRUM
(NC = No Change, D = Degraded, I = Improved, L = Lost)

Sample	Cell type	Area [cm^2]	ΔE_{ff} (%)	Remarks
Cell A	a-Si on stainless	816	9.14	I
Cell B	a-Si on stainless	816	10.01	I
Cell C	a-Si on Kapton (DuPont)	168	–37.08	D
Cell Da	a-Si	14	–94.76	D
Cell Db	a-Si	14	–99.18	L
Cell Dc	a-Si	14	–97.49	L
Cell Dd	a-Si	14	–95.98	L
Cell De	a-Si	14	–78.86	L
Cell Df	a-Si	14	–89.02	L
Cell E	CIGS with coating	180	26.57	I
Cell F	CIGS with coating	180	1.27	NC
Cell G	CIGS	17.5	97.88	I^{++}
Cell H	CIGS	63	–75.84	L
Cell I	a-Si	68	–68.81	D^{--}

Conclusions

The scaled parasitic current results reported in table A indicate that the large 618 cm^2 area a-Si cells A and B consistently returned the lowest and subsequently best leakage current figures, losing an average of two orders of magnitude less current than cells C, E, F, G, H, and I. The six individual cells (Da, Db, Dc, Dd, De, and Df) consistently returned the highest parasitic current results, losing on average three orders of magnitude more current, than either cells A or B. The parasitic current figures appear to be skewed and may be due to large scale edge effects acting on the smaller area cells.

At first glance the arcing threshold results in table B may look encouraging. Unfortunately, combining the arc threshold results with the findings from the PV solar array flash simulator laboratory in table C, paints an entirely different picture all together. For example, three of the six amorphous silicon cells (d, e, and f) individual cells in sample D were able to standoff up –400 V without arcing. In fact cells d, e, and f of sample D had the highest recorded arc threshold values for any of the cells tested in table (B). However table C shows that five of the six cells in sample D were lost after arc testing and one cell (Da) from the same group of cells survived but was badly degraded. Similarly, cell H was lost after arc testing and cells C and I were badly degraded. Additionally cells A, B, and G improved in efficiency after arc test in plasma whereas cell F showed no appreciable change.

So what does the above the compiled data mean? Why do some cells improve, while others degrade and why still other cells are lost entirely? First all CIGS and a-Si cells are not created equally. Particularly in the case of a-Si cells, the coatings are not completely uniform in thickness. The uniformity of the coating (thickness) may vary from point to point across the entire face of the insulating layer. Furthermore the coatings may also contain: voids, wrinkles, trapped air as well as both large and small (pinholes) scale defects, which are artifacts left over from the manufacturing process. With the previous two statements in mind an attempt will be made to describe why certain cells are lost. Obviously, something caused the cells to malfunction, resulting in a catastrophic loss of the cell as a direct consequence of plasma arc testing. Particularly for thin coatings, applied over an area of small dimensions, the cell will be even more perceptible to large potentials (and therefore large scale E-fields) than is the case for much larger cells having a greater surface area. For the same size arc, damage will scale according to the surface area, so smaller cells will incur more damage than larger cells. This appears to be the case of cells (a to f) in sample D. Now to the final question of why some cells degrade while others improve in efficiency after plasma arc testing. Generally speaking cell efficiency will depend on:

- The quality (uniformity of the insulating material) and who manufactures it. For example cells A and B, from the same manufacturer, improved while cells C and I supplied from a different manufacturer degraded.
- Large area a-Si cells appear to be less susceptible to arc damage caused by large scale bias potentials then is the case for smaller area a-Si cells. For example the two large area (816 cm^2) a-Si cells: A and B had improved efficiency after arcing in LEO, while the intermediate sized a-Si cells: C (168 cm^2) and I (63 cm^2) degraded after arcing.
- Arc damage in amorphous silicon cells appears to scale according to the surface area, so smaller cells will incur more damage than is the case for larger area cells. This appears to be the case of cells (a to f) in sample D.
- CIGS cell performance appears to depend less on large scale potentials and surface area effects then is the case for a-Si cells. For example CIGS cell G which is small in area (17.5 cm^2) had the largest gain in efficiency (97.88 percent) for any of the cells tested. The Intermediate sized CIGS cells E and F either improved in efficiency (Cell E) or stayed the same (Cell F) after arc testing.

In accordance with the designed array operating voltage (set by AFRL for arrays to be configured in arrays for space applications using the current a-Si and CIGS technologies) the expected magnitude of the plasma interactions between the cells and the LEO plasma environment calculated from equation (1) is –273 V. Inspection of table B shows that the only cells (b to f) in sample D, cells G, H, and I arced well above the specified –273 V limit. Unfortunately cells (b to f) in sample D and cell H were lost (cell I was degraded badly) after plasma arc testing. Only one cell (cell G) passed the –273 V limit. In retrospect other cells might have passed if the maximum limit of –273 V had been rigidly maintained throughout the experiment.

Finally the sustained arc tests with the SAS placed between cells E and F show that the pulse width on triggered arcs between adjacent cells is only about 30 μS in length. Because the arc pulse width is small no sustained arcs were detected. This is not surprising since the gap thickness between cells E and F is large being about 0.5 cm in length (fig. 6(a)). The sustained arc tests with the SAS placed between adjacent Strings 1 and 2 indicate that although some arc pulse widths are extended in length, they are not sustained because the current falls back to zero at the end of the current pulse (fig. 8(b)). Extended arcs may be considered precursors to sustained arcs which would have resulted if the gap thickness between cells had been smaller in dimension.

References

1. Vaughn, J.A., Carruth Jr., M.R., Katz, I., Mandell, M.J., and Jongeward, G.A., "Electrical Breakdown Currents on Large Spacecraft in Low Earth Orbit," Journal of Spacecraft and Rockets, vol. 31, no. 1, 1994.
2. Katz, I., Lilley, J.R., Greb, Macoy, J.E., Galofaro, J., and Ferguson, D.C., "Plasma Turbulence Enhanced Current Collection: Results from the Plasma Motor Generator Electrodynamic Tether Flight," Journal of Geophysical Research, vol. 100, no. A2, 1995.
3. Vayner, B.V., Ferguson, D.C., and Galofaro, J.T., Galofaro, "The Spacecraft Surfaces Degradation and Contamination Caused by Arcing in Low Density Plasmas," XVIII ISDEIV Conference, Eindhoven, Netherlands, Aug. 17–21, 1998.
4. Galofaro, J., Vayner, B., and Ferguson, D., "Electrical Breakdown of Anodized Coatings in Low Density Plasmas," Journal of Spacecraft and Rockets, vol. 36, no. 4, 1999.
5. Vayner, B., Galofaro, J., and Ferguson D., "Interactions of High-Voltage Solar Arrays with Their Plasma Environment: Ground Tests," Journal of Spacecraft and Rockets, vol. 41, no. 6, 2004.
6. Vayner, B., Galofaro, J., and Ferguson, D., "Interactions of High-Voltage Solar Arrays with Their Plasma Environment: Physical Processes," Journal of Spacecraft and Rockets, vol. 41, no. 6, 2004.

7. Granata, J.E., Sahistrom, T.D., Hausgen, P., Messenger, S.R., Walters, R.J., Lorentzen, J.R., "Thin-Film Photovoltaic Radiation Testing and Modeling for a MEO Orbit," Conference Record of the IEEE Photovoltaic Specialists Conference, Jan. 3–7, 2005, Lake Buena Vista, FL, pp. 607–610.
8. Galofaro, J., Vayner, B., Degroot, W., and Ferguson, D., "The Role of Water Vapor and Dissociative Recombination Process in Solar Array Arc Initiation," AIAA paper 2002–0938, 40th Aerospace Sciences Meeting and Exhibit, Jan. 14–17, 2002, Reno, Nevada.
9. Galofaro, J., Vayner, B., Ferguson, D., and Degroot, W., "A desorbed Gas Molecular Ionization Mechanism for Arcing Onset in Solar Arrays Immersed in a Low Density Plasma," AIAA Paper 2002–2262, 33rd Plasmadynamics and Lasers Conference, May 20–23, 2002, Maui, Hawaii.
10. Galofaro, J., Vayner, B., and Ferguson, D., "Daytime Solar Heating of Photovoltaic Arrays in a Low Density Plasmas," AIAA Paper 2003–4177, 34th Plasmadynamics and Lasers Conference, June 23–26, 2003, Orlando, Florida.
11. Galofaro, J., Vayner, B., and Ferguson, D., "On Orbit Daytime Solar Heating Effects: A Comparison of Ground Chamber Arc Results," NASA/TM—2004-212890, 8th Spacecraft Charging Conference, Huntsville, AL, October 20–24, 2003.

REPORT DOCUMENTATION PAGE

Form Approved
OMB No. 0704-0188

1. AGENCY USE ONLY (*Leave blank*)	2. REPORT DATE	3. REPORT TYPE AND DATES COVERED
	November 2006	Technical Memorandum

4. TITLE AND SUBTITLE

Experimental Results of Thin-Film Photovoltaic Cells in a Low Density LEO Plasma Environment: Ground Tests

5. FUNDING NUMBERS

WBS 22R–612–50–81–0414–01

6. AUTHOR(S)

Joel T. Galofaro and Boris V. Vayner

7. PERFORMING ORGANIZATION NAME(S) AND ADDRESS(ES)

National Aeronautics and Space Administration
John H. Glenn Research Center at Lewis Field
Cleveland, Ohio 44135–3191

8. PERFORMING ORGANIZATION REPORT NUMBER

E–15707

9. SPONSORING/MONITORING AGENCY NAME(S) AND ADDRESS(ES)

National Aeronautics and Space Administration
Washington, DC 20546–0001

10. SPONSORING/MONITORING AGENCY REPORT NUMBER

NASA TM—2006-214430

11. SUPPLEMENTARY NOTES

Prepared for the Fourth World Conference on Photovoltaic Energy Conversion sponsored by the Institute of Electrical and Electronics Engineers, Waikoloa, Hawaii, May 7–12, 2006. Joel T. Galofaro, Glenn Research Center; and Boris V. Vayner, Ohio Aerospace Institute, 22800 Cedar Point Road, Brook Park, Ohio 44142. Responsible person, Joel T. Galofaro, organization code, RPV, 216–433–2294.

12a. DISTRIBUTION/AVAILABILITY STATEMENT

Unclassified - Unlimited
Subject Category: 18

Available electronically at http://gltrs.grc.nasa.gov

This publication is available from the NASA Center for AeroSpace Information, 301–621–0390.

12b. DISTRIBUTION CODE

13. ABSTRACT ***(Maximum 200 words)***

Plasma ground testing results, conducted at the Glenn Research Center (GRC) National Plasma Interaction (N-PI) Facility, are presented for a number of thin-film photovoltaic cells. The cells represent a mix of promising new technologies identified by the Air Force Research Laboratory (AFRL) under the CYGNUS Space Science Technology Experiment (SSTE-4) Program. The current ground tests are aimed at characterizing the performance and survivability of thin film technologies in the harsh low earth orbital space environment where they will be flown. Measurements of parasitic current loss, charging/dielectric breakdown of cover-slide coatings and arcing threshold tests are performed for each individual cell. These measurements are followed by a series of experiments designed to test for catastrophic arc failure mechanisms. A special type of power supply, called a solar array simulator (SAS) with adjustable voltage and current limits on the supply's output, is employed to bias two adjacent cells at a predetermined voltage and current. The bias voltage is incrementally ramped up until a sustained arc results. Sustained arcs are precursors to catastrophic arc failure where the arc current rises to a maximum value for long timescales often ranging between 30 to 100 μsec times. Normal arcs by comparison, are short lived events with a timescale between 10 to 30 μsec. Sustained arcs lead to pyrolization with extreme cell damage and have been shown to cause the loss of entire array strings in solar arrays. The collected data will be used to evaluate the suitability of thin-film photovoltaic technologies for future space operations.

14. SUBJECT TERMS

Arcing; Solar array arcing; Sustained arcs; CIGS thin film; Amorphous silicon thin films

15. NUMBER OF PAGES

21

16. PRICE CODE

17. SECURITY CLASSIFICATION OF REPORT	18. SECURITY CLASSIFICATION OF THIS PAGE	19. SECURITY CLASSIFICATION OF ABSTRACT	20. LIMITATION OF ABSTRACT
Unclassified	Unclassified	Unclassified	